A Comparative Evaluation of Isolated Bi-directional DC/DC Converters with Wide Input and Output Voltage Range

F. Krismer, J. Biela, J. W. Kolar
Power Electronics System Laboratory
Swiss Federal Institute of Technology (ETHZ)
Zurich, Switzerland

***Abstract*— The working principles and design equations of four different isolated, bi-directional DC to DC converter topologies (a dual active bridge converter, a series resonant converter and two multiple stage topologies) for a 2kW bi-directional battery charger that can be operated in a wide input and output voltage range are presented in this paper. The results of a detailed mathematical analysis of the converter topologies as well as digital simulation results are used to select the most efficient topology for this specific converter application, where the two-stage series resonant converter is identified to be the most promising, with up to 90% efficiency at rated power.**

Keywords: converter design, modulation techniques, converter comparison, high current operation, high frequency conversion

I. INTRODUCTION

With the increasing need for electric power in future automobiles there is an increasing requirement for bi-directional isolated DC/DC converters to transfer energy between different voltage levels, such as between the low voltage accessories and the high voltage drive train. An alternative application for such type of converters is in future more-electric aircraft where the power converters will be used to interface between the aircraft power distribution bus and specific loads [1].

Numerous different topologies for isolated, bi-directional DC/DC converters have been previously described [2]-[5] but no comprehensive comparative evaluation of the systems has been presented in the literature so far.

In this paper four topologies of isolated, bi-directional converters (**Fig. 1**) are investigated and compared for the realization of a 2kW interface between a low voltage battery and a high voltage DC bus. The converters are referred to as topology DAB_1 and DAB_2 for the dual active bridge (DAB) converter and SRC_1 and SRC_2 for the series resonant converter (SRC) according to the caption of Fig. 1. All these converters allow an operation in a wide input and output voltage range. The actual operating range is depicted in **Fig. 2** where the battery voltage ranges from 11V to 16V (nominal voltage is 12V) and a voltage range of 220V to 447V is specified for the high voltage bus (nominal voltage is 336V). The minimum switching frequency is set to f_S = 100kHz which is a compromise between the size of the passive components and/or power density, and/or the amount of switching losses and conversion efficiency.

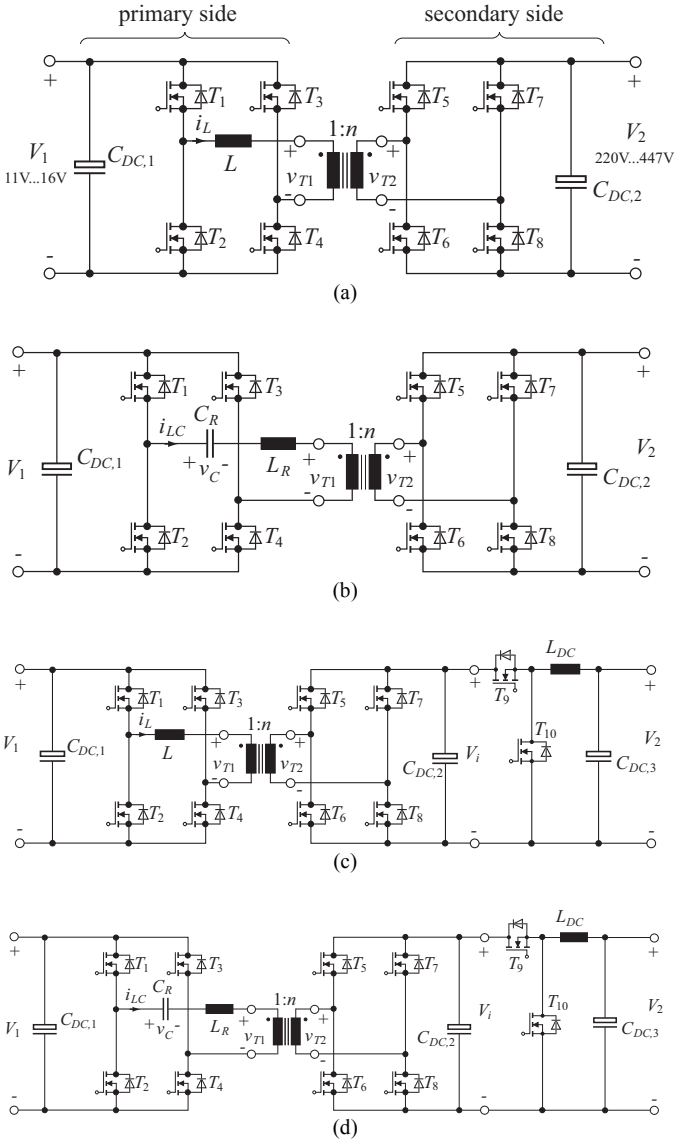

Figure 1. Isolated and bi-directional DC/DC converter topologies: (a) DAB_1: dual active bridge converter [2, 4], (b) SRC_1: series resonant converter [5], (c) DAB_2 and (d) SRC_2: two stage converters based on the combination of an isolation stage with a non-isolated voltage converter.

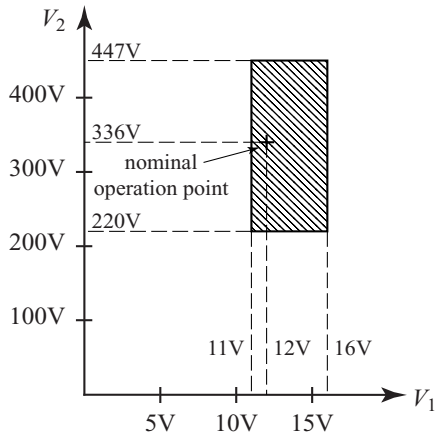

Figure 2. Operating range of the bi-directional DC/DC converter (hatched area) as defined by the input and output voltage ranges.

According to Fig. 1, all the topologies discussed in this paper comprise a similar isolation stage implemented with a full bridge converter on the primary side (low voltage side) and on the secondary side (high voltage side) of the transformer. Moreover, topologies DAB_1 and DAB_2 are based on the dual active bridge converter [2, 4] where full bridge circuits, which are used on the low voltage and high voltage side, facilitate freewheeling states. This represents an additional degree of freedom for the converter control, which is an advantage compared to half-bridge circuits. Also, the full bridge circuit is considered to be advantageous over a push-pull circuit for the specified power rating. The main drawbacks of push-pull circuits are the lower transformer utilization, the need for additional snubber circuitry for transistor blocking voltage limitation, and increased conduction losses because switches with higher voltage rating / on-resistance are required [6].

The dual active bridge converter (Fig. 1(a)) utilizes the leakage inductance L as a buck or boost inductor to cover the desired output voltage range [2]. Adding a capacitor in series to the leakage inductance leads to the series resonant converter (Fig. 1(b)) which can also be operated with bi-directional power flow within a wide range of input and output voltages [5]. Separating the voltage level conversion and isolation stages leads to topologies DAB_2 and SRC_2 with the voltage conversion stage being on the high voltage side. There, a degree of freedom is gained for the optimization of the converter control, as the level of the internal voltage V_i can be selected within a defined range. This allows for a reduction in the switch losses and the electrical stress on the transformer. However, additional power losses now occur in the voltage level converter.

Another category of bi-directional converters are topologies with a current-fed full bridge arrangement on the low voltage side. These converters have reduced rms switch and transformer current values [3] at the expense of higher voltage ratings of the switches. Additional circuitry is necessary to protect the switches from overvoltages, which occur due to the energy stored in the transformer leakage inductance and the DC choke. It is also difficult to manufacture an efficient high current DC choke [7]. Therefore, the voltage-fed topologies are considered to be advantageous over the current-fed topologies with respect to reliability and converter cost.

In this paper, **Section II** describes the working principle of the converters and a control scheme, which ensures minimum switching losses and minimum component stresses, is defined for each topology. In **Section III** the evaluation criteria, i.e. power losses of the switches, conduction losses of the passive components and copper and core losses of the transformer, are defined and applied to the converter topologies in **Section IV** based on the results gained from mathematical models and digital simulations. Finally, a comparison of the different converter concepts concerning efficiency and volume is given.

II. CONVERTER OPERATING PRINCIPLES AND DESIGN

A. Dual active bridge converter (topology DAB_1)

Depending on the control this converter can be used to generate an output voltage that is higher or lower than the transformed input voltage, i.e. the input voltage multiplied with the transformer turns ratio. Accordingly, the operating mode is denominated as step up or step down operation where bi-directional power flow is possible in both cases.

1) Converter modulation method

In [4] an extensive evaluation of the operation of this circuit for three different control techniques is given:

- rectangular operation mode with 50% duty cycle of the primary and secondary transformer voltages, v_{T1} and v_{T2}: allows for the highest power transfer with the given converter; zero voltage switching (ZVS) is only achieved within a defined range of the phase shift φ of v_{T1} and v_{T2}. Moreover, the instantaneous transistor currents that occur during the switching process can not be explicitly controlled. However, for the primary side full bridge of the bi-directional converter specified in Section I, low transistor currents during the switching time instant are compulsory in order to achieve low switching losses. Therefore, this modulation scheme is not considered as appropriate for the given converter.
- triangular current mode (**Fig. 3**(a1) and 3(a2)): the duty cycle of either the primary or the secondary transformer voltage is smaller than 50%; allows for lowest switching losses [4]
- trapezoidal current mode (Fig. 3(a3)): the primary and the secondary full bridge converters apply voltages v_{T1} and v_{T2} with a duty cycle smaller than 50% to the transformer. Compared to the triangular current mode, a higher power transfer is possible for a given converter.

High rms and peak currents on the primary side of the power converter specified in Section I represent the biggest challenge in its implementation. Therefore, a modulation scheme is chosen that allows for an optimization of the primary side rms current values within the defined range of input and output voltages V_1 and V_2. Additionally, a defined limit of the primary side transistor currents should not be exceeded during the switching instants in order to achieve low switching losses. These suppositions are accomplished with the triangular and the trapezoidal current mode modulation scheme.

The triangular current mode modulation (Fig. 3(a1), 3(a2)) allows for pure zero current switching (ZCS) on the primary side and combined ZCS/ZVS on the secondary side, which is achieved

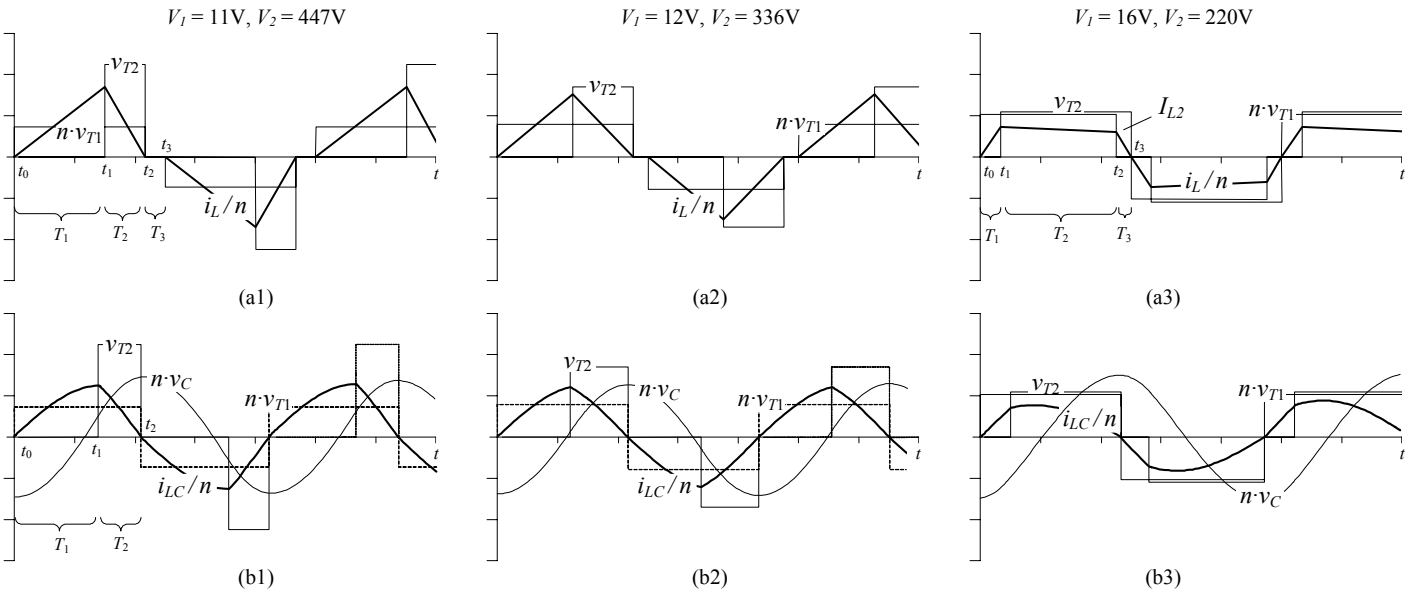

Figure 3. Simulated waveforms for secondary side referred transformer current $i_L(t) / n$ respectively $i_{LC}(t) / n$, transformer voltages $n \cdot v_{T1}(t)$ and $v_{T2}(t)$, and the resonant capacitor voltage $n \cdot v_C(t)$ for the dual active bridge converter DAB_1 ((a1) to (a3)) and the series resonant converter (topology SRC_1, (b1) to (b3)). Different operating points at 2kW output power are shown for energy flowing from the low voltage (primary) to the high voltage (secondary) side. Input and output voltages specified on top of this figure apply to all waveforms of the belonging column; time scale: 2µs/Div., voltage scale: 200V/Div., and current scale: 20A/Div.

for a transformer turns ratio n of

$$n < \frac{V_{2,\min}}{V_{1,\max}} \,. \tag{1}$$

Figures 3(a1) and 3(a2) depict the transformer current and voltage waveforms according to a power transfer from the primary to the secondary side. There, at time instant t_0, only the primary voltage V_1 is applied to the transformer which causes the transformer current to rise. At time instant t_1 the secondary side full bridge is turned on with $v_2(t_1) = V_2$ and the transformer current decreases again[a] until it reaches zero at t_2. For constant frequency control, a dead time interval T_3 may be inserted to adjust the amount of transferred power. With variable frequency control the time interval T_3 is zero. At time instant t_3 the next half cycle starts. The direction of the power transfer is reversed, when time intervals T_1 and T_2 are transposed.

The limitation of the transformer turns ratio n from (1) leads to an ineffective utilization of the secondary side components of the converter. This limitation can be circumvented with trapezoidal current mode modulation (Fig. 3(a3)) by allowing a certain switch current $I_{L2} = i_L(t_2)$ at time instant t_2. The waveforms for transformer current i_L and voltages v_{T1} and v_{T2} in Figure 3(a3) again correspond to a power transfer from the low voltage side to the high voltage side. Time intervals T_1 and T_2 are identical to those of the triangular current mode modulation except that the transformer current i_L is greater than zero at time instant t_2. There, the primary side full bridge applies $v_1(t_2) = 0$V to the transformer and the transformer current decreases until it reaches zero at t_3.

Equation (2) is used to determine the amount of transferred power for the trapezoidal current mode modulation depending on the given switching frequency f_S, primary and secondary DC voltages V_1 and V_2, the turns ratio n of the transformer, the value of the converter inductor L, and the primary side transistor current I_{L2} at the switching time instant t_2 (Fig. 3(a3)). The first term in the sum of this expression describes the transferred power for the triangular current mode modulation ($I_{L2} = 0$). Obviously, no power can be transferred with the triangular current mode modulation for $n \cdot V_1 = V_2$. The second and the third part of (2) are due to the trapezoidal current mode modulation.

$$P = \frac{V_1 \cdot \left(\frac{V_1 \cdot (V_2/n - V_1)}{4 L f_S} + I_{L2} \frac{n V_1^2}{V_2} - L f_S I_{L2}^2 \cdot \left(\left(\frac{n V_1}{V_2} \right)^2 + \frac{n V_1}{V_2} + 1 \right) \right)}{V_2 / n} \,. \tag{2}$$

2) Converter converter design

The proposed design method is based on the converter specifications presented in Section I. Moreover, the maximum switch current $I_{L2} = i_L(t_2)$ is taken into consideration in order to achieve low switching losses on the primary side.

The evaluation of the transformer turns ratio n and inductor value L is an iterative process that starts with the selection of n. Thereafter a condition for the minimum value for the inductor L which is necessary to fulfil the above mentioned requirements is derived from (2),

$$L < L_{\min} = \frac{I_{L2} V_1^3 \frac{V_2}{n} - P \left(\frac{V_2}{n} \right)^3 + \left(\frac{V_2}{n} \right)^2 \sqrt{I_{L2}^2 V_1^3 \left(\frac{V_2}{n} \right) - 2 P I_{L2} V_1^3 + P^2 \left(\frac{V_2}{n} \right)^2}}{2 f_S I_{L2}^2 V_1 \cdot \left(V_1^2 + \frac{V_1 V_2}{n} + \left(\frac{V_2}{n} \right)^2 \right)} \,. \tag{3}$$

This procedure enables a search for a combination of values for the transformer turns ratio n and inductor L that results in a minimum rms transformer current for the specified input and output voltage range.

B. Series resonant converter (topology SRC_1)

Also the series resonant converter (Fig. 1(b)) can be operated with bi-directional power flow. In [5] the working principle of this circuit is described for a modulation scheme similar to the

[a] assuming that condition (1) is fulfilled

rectangular modulation scheme described for the DAB. However, a different modulation scheme is investigated here that provides an improvement in the utilization of the primary side converter components.

1) Converter modulation method

A modulation scheme similar to triangular current mode modulation for the DAB can be applied with variable switching frequency to the series resonant converter. This enables pure ZCS on the primary side, and combined ZVS/ZCS on the secondary side, and allows for an efficient utilization of the primary side switches. There, the low voltage side switches are operated with 50% duty cycle with the switching time instant at the zero crossing of the resonant current ($t = t_0$ and $t = t_2$ in Fig. 3(b1)). For the case of power flowing from the primary to the secondary side, only the primary voltage V_1 is applied to the transformer during time interval T_1 and the resonant current starts to increase according to Figure 3(b1). As the converter is operated above its resonance frequency f_0, the voltage V_2 is applied to the secondary side of the resonant circuit at time instant $t_1 < 1/(2f_0)$. For a transformer turns ratio of

$$n < n_0 = \frac{V_{2,\min}}{V_{1,\max}}, \tag{4}$$

the resonant current $i_{LC}(t)$ is finally forced back to zero at time instant t_2. In steady state operation, the duty cycle of the secondary side converter stage is derived as

$$D = \frac{T_2}{T_{12}} = \frac{1}{2} + \frac{1}{2\pi \cdot f_0 \cdot T_{12}} \cdot \arcsin\left(\frac{\left(2V_1 - \frac{V_2}{n}\right) \cdot \sin(T_{12} \cdot \pi \cdot f_0)}{\frac{V_2}{n}} \right), \tag{5}$$

with $T_{12} = T_1 + T_2$. Again, the direction of power transfer is reversed when the time intervals T_1 and T_2 are transposed.

2) Converter design

In addition to the specifications given in Section I, minimum and maximum switching frequency ($f_{S,\min}$ and $f_{S,\max}$) at full power operation are required to carry out the design method proposed in this paper.

First of all, the transformer turns ratio is selected in order to meet condition (4). A suggested value of n close to n_0 improves the utilization of the secondary side. In a second step the resonance frequency is set to a temporary value below the minimum switching frequency,

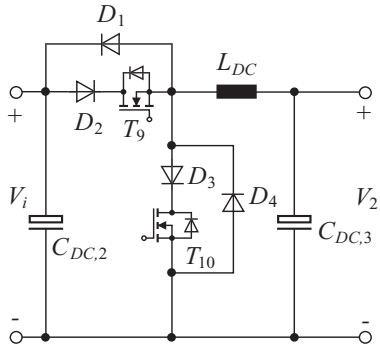

Figure 4. Voltage level converter with $V_2 \leq V_i$. Realization is based on silicon carbide Schottky diodes for improved switching performance.

$$f_{0,temp} = 0.8 \ldots 0.9 \cdot f_{S,\min}. \tag{6}$$

Together with (5) and the expression for the transferred power,

$$P = \frac{V_1 \cdot \left(V_1 \cdot (1 - \cos(2\pi f_0 \cdot T_{12})) - \frac{V_2}{n} \cdot (1 - \cos(2\pi f_0 \cdot T_2)) \right)}{\pi f_0 \cdot T_{12} \cdot Z_0 \cdot (1 + \cos(2\pi f_0 \cdot T_{12}))}, \tag{7}$$

this enables one to numerically solve for the steady state switching frequency at a given operating point. This in turn allows to search for the characteristic impedance Z_0 of the series resonant circuit needed to achieve the desired frequency ratio $f_{S,\min}/f_{S,\max}$. Finally, the switching frequency is adjusted to

$$f_0 = f_{0,temp} \cdot \frac{f_{S,\min,num}}{f_{S,\min,desired}}, \tag{8}$$ [b]

with the numerically evaluated minimum switching frequency $f_{S,\min,num}$ and the desired minimum switching frequency $f_{S,\min,desired}$.

C. Two stage topologies (topologies DAB_2 and SRC_2)

The requirement for the converter to be operated within a wide input and output voltage range results in operation regions of inefficient switch and transformer utilization. Therefore, a two stage solution is considered which consists of two separate conversion stages: an isolation stage and a non-isolated voltage converter. Initially four different possibilities were investigated:

1. primary side voltage converter with $V_1 < V_i$
2. primary side voltage converter with $V_1 > V_i$
3. secondary side voltage converter with $V_i < V_2$
4. secondary side voltage converter with $V_i > V_2$

Low conversion efficiency is expected for the primary side voltage converters (concepts 1 and 2) (below 85% for the boost converter in [7] operated with an output power of 2kW). The third concept seems to be promising, however only inefficient semiconductor switches are available for the resulting voltage range of V_i. Therefore, the last proposal was investigated more detailed.

1) Converter design

The most efficient operation of the converters DAB_1 and SRC_1 is achieved for the primary voltage V_1 being close to the reflected secondary voltage V_2/n. Moreover, the proposed modulation method for topology SRC_1 only allows for $V_2 > V_1 \cdot n$ and also the discussed method for topology DAB_1 primarily suggests that kind of operation.

In order to achieve a balanced utilization of the two converter stages, it is proposed that either the isolation stage is operated with an amplification $v_1 \geq v_{1,0}$ or that the non-isolated voltage converter is operated with $v_2 \leq 1$,

$$\left.\begin{aligned} v_1 &= v_{1,0} \\ v_2 &= \frac{V_2}{V_i} \end{aligned}\right\} \quad \frac{V_2}{V_1} < v_{1,0}, \tag{9}$$

$$\left.\begin{aligned} v_1 &= \frac{V_i}{V_1} \\ v_2 &= 1 \end{aligned}\right\} \quad \frac{V_2}{V_1} \geq v_{1,0}, \tag{10}$$

[b] The switching frequency $f_S = 1/(2 \cdot T_{12})$ is directly proportional to the resonance frequency f_0 in (5) and (7).

where $v_{1,0}$ is the voltage transformation ratio of the isolation stage needed for maximum input and output voltage,

$$v_{1,0} = \frac{V_{2,\max}}{V_{1,\max}}, \tag{11}$$

v_1 the amplification of the isolation stage,

$$v_1 = \frac{V_i}{V_1}, \tag{12}$$

and v_2 the amplification of the non-isolated voltage converter

$$v_2 = \frac{V_2}{V_i}. \tag{13}$$

With this, the transistors are utilized up to the maximum operating voltage in order to reduce the secondary side currents.

The non-isolated voltage converter stage is realized according to **Figure 4**. Silicon carbide Schottky diodes (D_1 to D_4) are used to achieve low switching losses. The designed values for the components of all converters are summarized in **Table I**.

III. COMPARISON OF CONVERTER TOPOLOGIES

For comparing the different converter systems key quantities such as converter efficiency and volume are taken into consideration.

A. Power losses of active and passive components

The conduction losses of all active and passive components are considered as a significant part of the total converter power loss. Other important sources of power loss are the transformer and the low voltage side PCB which carries high currents.

The MOSFET conduction losses are calculated based on the on resistance $R_{DS,on}$ and the energy stored in the parasitic capacitors is used to evaluate the losses due to ZCS. For ZVS the inductive turn off losses are considered and are experimentally estimated for the primary side transistors at given switch voltage V_{DS} and current I_D,

$$E_{off} = \frac{V_{DS} \cdot I_D}{2} \cdot 500\text{ns}, \tag{14}$$

for transistor currents $I_D < 100$A. For the secondary side inductive turn off switching losses, the given datasheet values for V_{DS} = 350V were scaled with the applied switch voltage,

$$E_{off} = E_{off,Datasheet}(350\text{V}, I_D) \cdot \frac{V_{DS}}{350\text{V}}. \tag{15}$$

TABLE I. CALCULATED CONVERTER COMPONENT VALUES

Top.	Single Stage Converters			Two Stage Converters		
	L, L_R	C_R	n	L, L_R	C_R	n
DAB_1, DAB_2	63nH	–	13	40nH	–	21
SRC_1, SRC_2	212nH	16µF	12	161nH	25µF	25

Finally, the switching losses for the non-isolated voltage converter in topologies DAB_2 and SRC_2 are calculated with the measurement data given in [8].

Power losses of the DC capacitors C_{DC} are calculated with the currents being approximated with the fundamental component at a frequency of 200kHz,

$$P = R_{ESR} I_{RMS}^2 \approx \frac{I_{RMS}^2}{2\pi \cdot 200\text{kHz} \cdot C \cdot \tan(\delta(200\text{kHz}))}; \tag{16}$$

for the resonant capacitor C_R a frequency of 100kHz is considered. For the DC choke L_{DC} the dissipated power is calculated with the rms current value and the DC resistance of the choke,

$$P = R_{DC} I_{RMS}^2. \tag{17}$$

Since the resonant inductor L_R is integrated into the transformer, its power losses are considered as part of the transformer losses. The auxiliary power supply accounts for a fixed amount of 20W power loss.

The converter efficiency is calculated with the total dissipated power P_{loss} and the output power P_{out} of the converter

$$\eta = 1 - (P_{loss} / P_{out}). \tag{18}$$

B. Transformer losses

The estimation of the transformer power losses is split into the winding losses (including HF losses) and the losses dissipated in the transformer magnetic core.

1) Winding losses

For the numeric calculation an interleaved arrangement of the primary and the secondary winding (S-P-S) is assumed, which consists of copper foils with the same width w as the transformer winding area. Moreover, the number of turns N is already defined by the converter design and it is the same as the number of copper foil layers p: $p = N$. Then, the overall winding losses can be minimized for a given current waveform with DC component I_{DC} and harmonic components I_n by optimizing the thickness d of the copper foil (one dimensional approximation, [9, 10], δ_0 is the skin depth at the fundamental frequency of the current)

$$d_{opt} = \delta_0 \cdot \sqrt[4]{\frac{15}{5p^2 - 1}} \cdot \sqrt[4]{\frac{I_{DC}^2 + \sum_{n=1}^{\infty} I_n^2}{\sum_{n=1}^{\infty} n^2 I_n^2}}. \tag{19}$$

With this, an effective winding resistance and the winding losses for all the given current waveforms can be calculated as

$$P_{Wdg,opt,p} = \frac{4}{3} \cdot R_{DC,opt,p} \cdot I_{RMS}^2 \quad \text{with} \quad R_{DC,opt,p} = \frac{N \cdot l_w}{\sigma \cdot w \cdot d_{opt}}. \tag{20}$$

With (20) the losses in the primary ($P_{Wdg,opt,p}$) and in the secondary winding ($P_{Wdg,opt,s}$) are calculated and added to determine the total winding losses

$$P_{Wdg,opt} = P_{Wdg,opt,p} + P_{Wdg,opt,s}. \tag{21}$$

2) Core losses

The transformer core losses are calculated using

$$P_{Core,p} = \frac{V_{Core}}{2} \cdot \frac{k_i (\Delta B)^{\beta-\alpha}}{T} \sum_j \left| \frac{V_{j,p}}{N_p A_C} \right|^{\alpha} (\Delta t_j) \qquad (22)$$

$$with \quad \Delta B = \sum_j \left| \frac{V_{j,p}}{N_p A_C} \right| (\Delta t_j)$$

which is a simplified expression for the improved general Steinmetz equation (iGSE) proposed in [11] and valid for flux waveforms with no minor loops (i.e. monotonic waveforms) as given for the compared converter topologies. There, the voltage waveform is given as a piecewise linear waveform V_j that is constant during the time intervals Δt_j. It is used for calculating the rate of change of the flux density and the peak to peak amplitude of the flux density ΔB. (A_C represents the core cross section area and V_{Core} the core volume; k_i, α, and β are called Steinmetz coefficients which can be calculated with information from the datasheet).

The total core losses $P_{Core} = P_{Core,p} + P_{Core,s}$ are calculated assuming that in half of the core volume the flux is linked with the primary winding and in the other half with the secondary winding. This is an approximation of the actual flux distribution which is accurate enough for the considered comparison of converter topologies.

C. *Low voltage side PCB power loss*

High rms currents (up to 200A) with a fundamental frequency of more than 100kHz on the primary converter side lead to significant ohmic power loss in the PCB, therefore the layout of the primary converter side is investigated separately. Low parasitic inductance and well distributed currents are achieved with a four layer PCB with the current planes on top of each other and the semiconductors being placed at the left and at the right borders of the PCB (**Fig. 5**).

Information about the current distribution is obtained from FEA simulation (Fig. 5). High current densities appear at the outer borders where the semiconductors are located. Therefore, additional layers are used to increase the copper thickness close to the transistors for the hardware realization of the converter. The power loss from this simulation amounts 23.36W for a rms current of 200A, and this corresponds to an equivalent resistance of $R = 0.58\text{m}\Omega$.

IV. CONVERTER EVALUATION

The power converters, which have been designed in Section II, are evaluated based on the methods described in Section III. The calculated current and voltage ratings for the switches suggest MOSFET semiconductors to be most suitable. The DC link capacitors C_{DC} are chosen such that the peak to peak capacitor voltage ripple is less than 5% of the minimum DC voltage. The boost inductor L_{DC} is chosen to achieve a peak to peak inductor current ripple below 2A. The design leads to the following component values for the converters:

- Primary side switches: $R_{DS,on}$ = 3mΩ/2 (two IRF2804S in parallel, $T_{junction}$ = 150°C)
- Secondary side switches: $R_{DS,on}$ = 150mΩ (CoolMOS SPW47N60C3, $T_{junction}$ = 150°C)
- Silicon carbide diodes, voltage level converter: V_F = 1.8V
- Primary side DC capacitor: $C_{DC,1}$ = 800µF, R_{ESR} = 111µΩ
- Secondary side DC capacitors: $C_{DC,2}$ = 3µF, R_{ESR} = 880µΩ and $C_{DC,3}$ = 470nF with R_{ESR} = 5.3mΩ

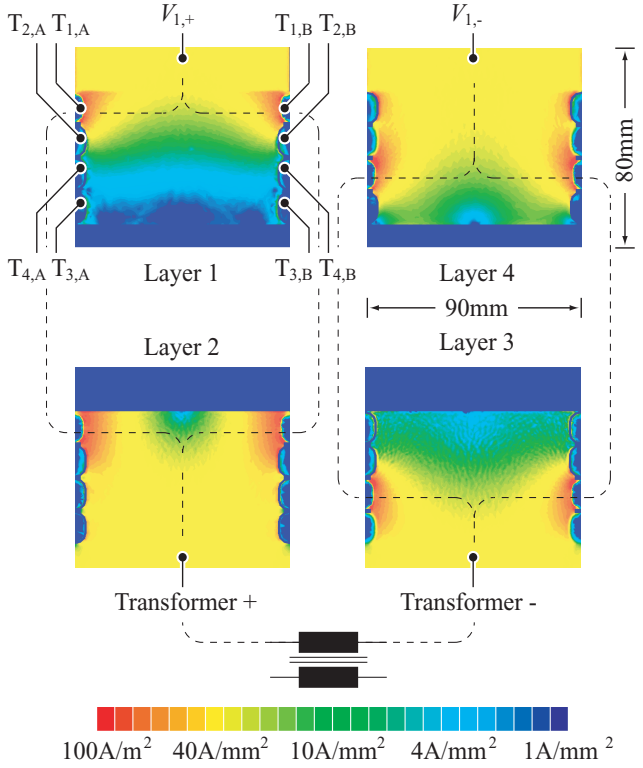

Figure 5. Current distribution in the primary side PCB for a sinusoidal current at the peak value of 283A and with a frequency of 100kHz flowing through transistors T_1 and T_4 ($T_{i,A}$ and $T_{i,B}$ denote the parallel disposition of two transistors forming T_i; the dashed line represents the current path). High current densities (red) occur at the borders where the transistors are located.

- Equivalent series resistance of the resonant capacitors for topologies SRC_1 and SRC_2: $R_{ESR,1}$ = 45mΩ, $R_{ESR,2}$ = 72mΩ
- Boost inductor in topologies DAB_2 and SRC_2: L_{DC} = 560µH, R_{DC} = 90mΩ, core: ELP64 ferrite core / EPCOS
- Transformer core: ELP64 / EPCOS

The calculated values for the leakage inductances, the resonant components and the transformer turns ratios are summarized in Tab. I.

For converter topology DAB_1 and the isolation stage of DAB_2 operation with constant switching frequency (f_S = 100kHz) as well as with variable switching frequency ($f_S \geq$ 100kHz) is investigated. For the series resonant converter only the operation with variable switching frequency ($f_S \geq$ 100kHz) is considered. The non-isolated voltage converters of the two stage topologies are operated with constant switching frequency (f_S = 100kHz).

Fig. 6(a) to (e) depict the calculated total power loss of the converters within the specified range of input and output voltages. There the DAB shows the highest total power losses when operated with constant switching frequency (Fig. 6(a)) which is due to high rms switch and transformer currents. A reduction of the power losses is achieved with variable switching frequency operation of the DAB (Fig. 6(b)). Further improvements are attained with the series resonant converter as reduced rms values of switch and transformer currents are achieved (Fig. 6(c)). However, the transformer turns ratios n of the single stage topologies DAB_1 and SRC_1 are smaller than those of the two stage topologies DAB_2 and SRC_2 as explained in Section II. Therefore, the two stage solutions not only allow for an optimized utilization

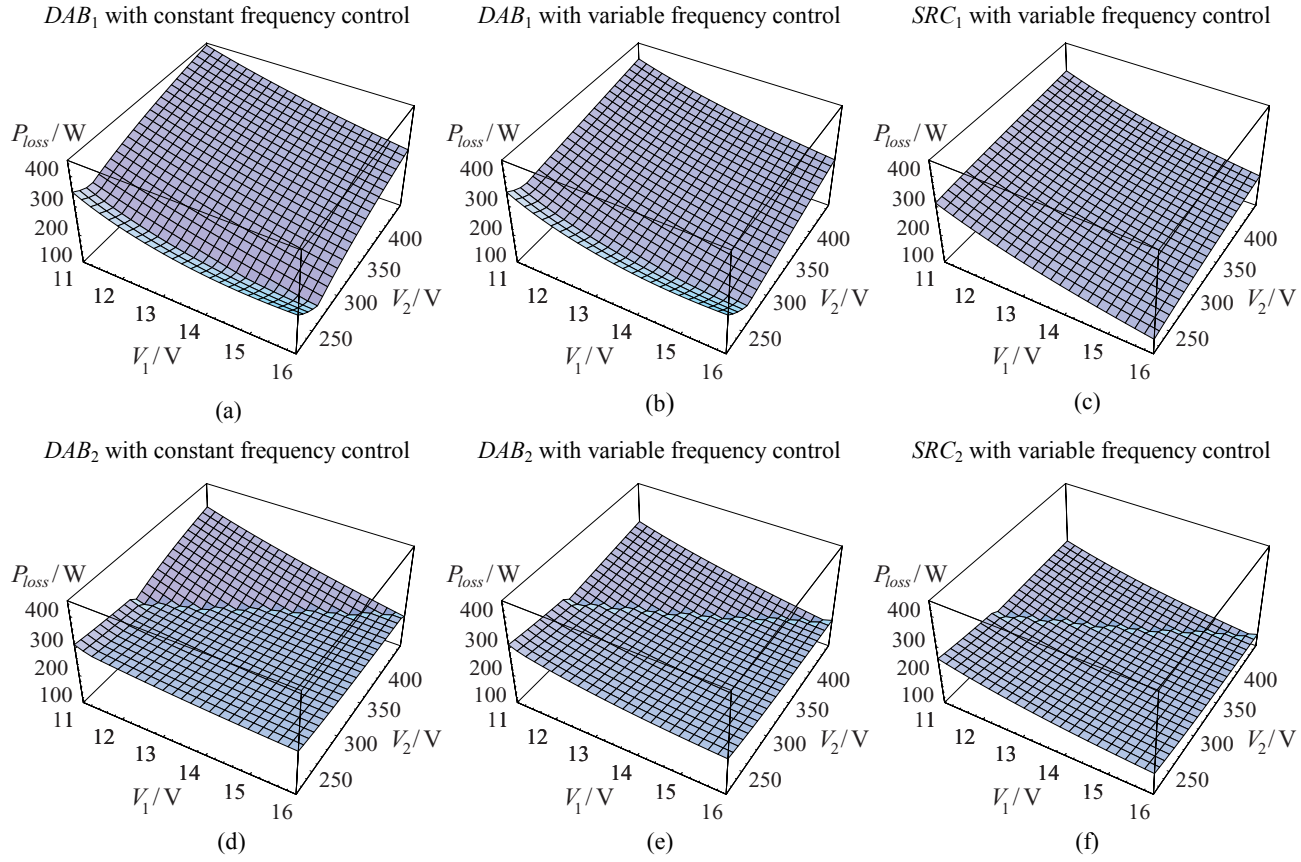

Figure 6. Calculated total power losses of the single stage ((a), (b), and (c)) and two stage converter topologies ((d), (e), and (f)) for P_{out} = 2kW.

of the isolation stage within a wide range of input and output voltages. Even more, the increased transformer turns ratio results in reduced secondary side rms current values, which in turn leads to decreased power losses (Fig. 6(d), (e), and (f)). The discontinuity that can be observed in these figures is due to the switching losses of the non-isolated voltage conversion stage which is operated according to (9) and (10). Therefore, the voltage converter stage is operated without switching in the region where a high voltage transfer ratio is needed and thus no switching losses occur.

Fig. 7 summarizes the calculated efficiency of the considered converter topologies for varying output power P_{out} at V_1=12V and V_2=336V. Obviously, a more effective converter utilization is achieved with variable frequency modulation for the high power range (P_{out} > 750W). However, the switching frequency increases for the variable frequency control method with decreasing output power which in turn causes significant switching losses at low output power (P_{out} < 750W). For the series resonant converter a gain in efficiency of 5% at rated power (from 85% to 90%) is achieved with the two stage topology. The additional voltage converter stage also increases the efficiency of the dual active bridge by 4% (from 84% to 88% at rated power) when variable frequency control is used.

The mathematical models that are derived in order to obtain the transistor and transformer current values needed for the analysis are verified with the use of digital simulation. **Figure 8** depicts the calculated as well as the simulated distribution of the power losses of the worst case (topology DAB_1 operated with constant switching frequency) and the best case (topology SRC_2 operated with variable switching frequency) for a power transfer

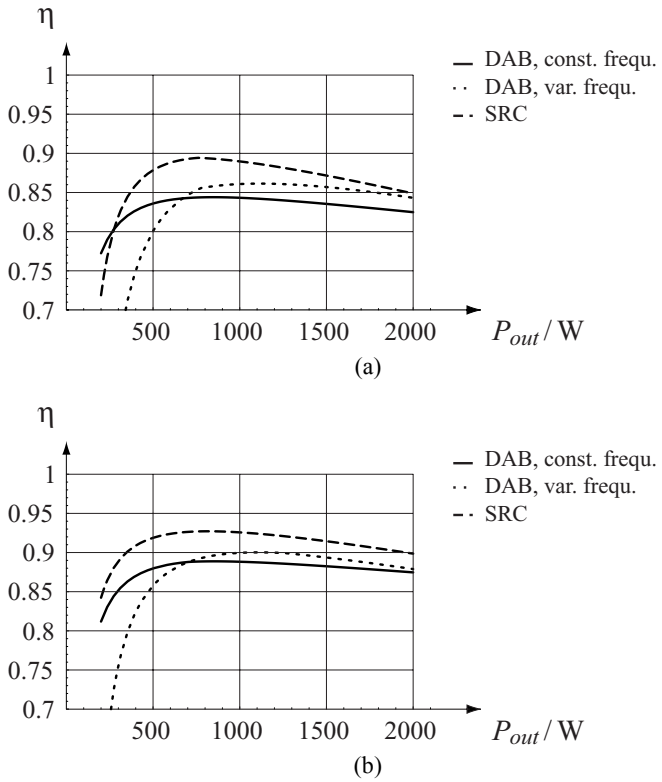

Figure 7. Calculated efficiency of the single stage (a) and two stage (b) converters at V_1=12V and V_2=336V depending on the output power.

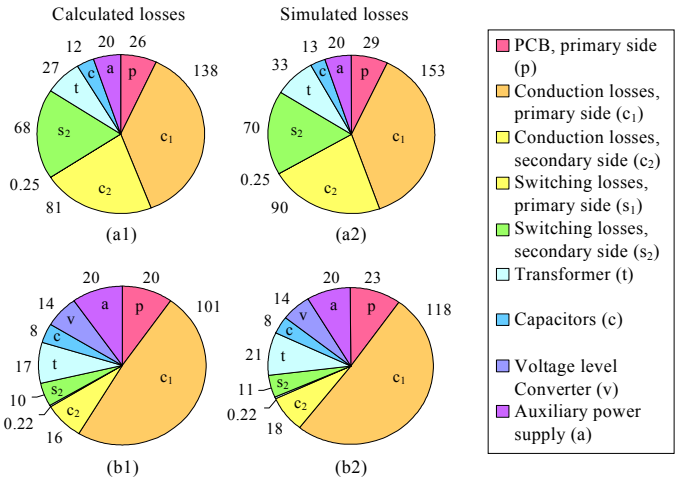

Figure 8. Calculated and simulated power loss distribution (in Watts) for nominal operation (V_1 = 12V, V_2 = 336V, P_{out} = 2kW) of topology DAB_1 operated at constant frequency ((a1), (a2)) and topology SRC_2 ((b1), (b2)). Power transfer from the primary to the secondary side is considered.

direction from the primary to the secondary side. It can be observed that the dominant part of the power losses is due to the conduction losses of the primary side transistors which justifies why the proposed design methods emphasize on the high current side. High conduction losses occur in the secondary side transistors of topology DAB_1 (Fig. 8(a1) and 8(a2)) because of a low transformer turns ratio n. Moreover, significant switching losses are observed on the secondary side of this single stage topology due to high peak currents at turn off. Compared with this, the two stage solution allows for a great reduction of the secondary side switching and conduction losses of the isolation stage.

Additional amount of dissipated power seen from the simulations (Fig. 8(b1) and 8(b2)) is due to the fact that the converter also has to transfer the power losses and this is neglected in the mathematical models.

Table II summarizes the volume which is needed for each converter. The volume of the electronics for the dual active bridge is taken from an actual hardware design of a 2kW converter. It includes the primary and the secondary side full bridges, the gate drivers, the transformer, the DC capacitors and the space needed for the auxiliary power supply. Additional volume is required for the series resonant capacitor C_R of topology SRC_1 and SRC_2 (V_{CR1} = 0.05dm^3 and V_{CR2} = 0.01dm^3 respectively) and for the voltage level converter of topologies DAB_2 and SRC_2 which consists of its electronics (V = 0.04dm^3) and the inductor L_{DC} (V_{LDC} = 0.065dm^3). However, a significant amount of volume is needed for the heat sink depending on the dissipated heat. The volume given in Table II is calculated based on the maximum dissipated power and a maximum tolerated difference between ambient and heat sink temperature of ΔT=60°C for a commercial heat sink with forced convection (8x8cm^2 cross section, R_{th} = 0.17 K/W for a length of l = 150cm). Obviously a reduction of the total converter volume is achieved with the two stage solution which is due to the improved efficiency.

TABLE II. CONVERTER VOLUME (IN DM^3) FOR 2KW OUTPUT POWER

	Topology and control method					
	***DAB*$_1$/ CF**	***DAB*$_1$/ VF**	***SRC*$_1$/ VF**	***DAB*$_2$/ CF**	***DAB*$_2$/ VF**	***SRC*$_2$/ VF**
Isolation stage	0.45	0.45	0.5	0.45	0.45	0.46
Non-isolated converter	–	–	–	0.105	0.105	0.105
Heatsink	1.46	1.26	1.13	1.13	0.93	0.66
Total volume	1.91	1.71	1.63	1.69	1.49	1.23

CF … constant frequency modulation, VF … variable frequency modulation

V. CONCLUSIONS

Four different topologies of bi-directional power converters with 2kW rated power, a primary voltage range of 11V to 16V, and a secondary voltage range of 220V to 447V are investigated: a dual active bridge and a series resonant converter, each of them also operated in combination with a separate voltage converter stage. With the presented design methods and modulation techniques, high switching frequency is achieved as well as high current operation on the primary converter side. From the converter analysis it follows, that the operation within a wide voltage range leads to a performance degradation for both, the DAB and the series resonant converter. It was shown that a reduced amount of total losses and a reduction of the converter volume can be achieved with a two stage topology as it enables high efficiency operation of the voltage conversion stage. There, the series resonant converter supported by a voltage level converter stage (topology SRC_2) is most promising with respect to converter efficiency and volume. Measurement results from an actual realization of the hardware will be presented shortly in order to validate the theoretical results.

VI. REFERENCES

[1] A. Julian, D. M. Divan, T. A. Lipo, F. Nozari, P. A. Mezs, "Double bridge resonant DC link converter with variable input and output frequency", Applied Power Electronics Conference and Exposition, vol. 1, pp. 181-186, March 1996.

[2] J. Walter, R. W. De Doncker, "High-power galvanically isolated DC/DC converter topology for future automobiles", IEEE 34th Annual Power Electronics Specialists Conference, vol. 1, pp. 27-32, June 2003.

[3] L. Zhu, X. Xu, F. Flett, "A 3kW isolated bi-directional DC/DC converter for fuel cell electric vehicle application", Proceedings of power electronics, pp. 77-82, June 2001.

[4] N. Schibli, "Symmetrical multilevel converters with two quadrant DC-DC feeding", EPFL, Thèse Nr. 2220, pp. 99-171, 2000.

[5] Y. Cheron, Soft commutation, technical edition. London: Chapman & Hall, 1992, pp. 208-219.

[6] A. Levy, "Comparing the push-pull, forward converter and full bridge topologies in low voltage, high power DC-DC converter", High Frequency Power Converter Conference (HFPC) proceedings, pp. 470-476, September 2001.

[7] M. B. Gerber, "On packaging techniques for a high power density DC/DC converter", M.Sc. thesis Johannesburg, South Africa: Rand Afrikaans Univ., Dec. 2001.

[8] J. Miniböck, J. W. Kolar, "Experimental analysis of the application of latest SiC diode and CoolMOS power transistor technology in a 10kW three-phase PWM (VIENNA) rectifier.", Power Electronics Conference (PCIM) proceedings, pp. 121-125, June 2001.

[9] P. L. Dowell, "Effect of eddy currents in transformer windings", IEE Proc., vol. 113, no. 8, pp. 1387-1394, August 1966.

[10] W. G. Hurley, E. Gath, J. G. Breslin, "Optimizing the AC resistance of multilayer transformer windings with arbitrary current waveforms", IEEE Transactions on Power Electronics, vol. 15, pp. 369 - 376, March 2000.

[11] J. Reinert, A. Brockmeyer, R. W. De Doncker, "Calculation of losses in ferro- and ferrimagnetic materials based on the modified Steinmetz equation", IEEE Transactions on Industry Applications, vol. 37, pp. 1055 - 106, July-August 2001.